Depth of Field Extension in Time-of-Flight Imaging

A Project Report

submitted by

SAGAR HONNUNGAR

in partial fulfilment of the requirements

for the award of the degree of

BACHELOR OF TECHNOLOGY

DEPARTMENT OF Electrical Engineering
INDIAN INSTITUTE OF TECHNOLOGY MADRAS.

May 2016

THESIS CERTIFICATE

This is to certify that the thesis titled Depth of field extension in time-of-flight imaging, submitted by **Sagar Honnungar**, to the Indian Institute of Technology, Madras, for the award of the degree of **Bachelor of Technology**, is a bona fide record of the research work done by him under my supervision. The contents of this thesis, in full or in parts, have not been submitted to any other Institute or University for the award of any degree or diploma.

Prof. Kaushik Mitra
Research Guide
Assistant Professor
Dept. of Electrical Engineering
IIT Madras, 600 036

Place: Chennai

Date: 1 May, 2016

ACKNOWLEDGEMENTS

I would like to express my deepest gratitude to my advisor Prof Kaushik Mitra for his constant support, encouragement and constructive feedback while working on this project. His enthusiasm and active involvement definitely helped me deliver my best in this work.

I am also thankful to Adithya Kumar Pediredla, Jason Holloway and Prof. Ashok Veeraraghavan from Rice University for collaborating with us on this project and providing us with the hardware data. The discussions I had with them gave me valuable insights during various stages of this project.

My friends and family have been extremely supportive and understanding during this project and also throughout the last four years. I am indebted to them for their love and support.

ABSTRACT

KEYWORDS: Time-of-flight imaging; lock-in correlation sensors; focal sweep; deblurring; depth of field extension

Time-of-flight (ToF) imaging is an active method that utilizes a temporally modulated light source and a correlation-based (or lock-in) imager that computes the round-trip travel time from source to scene and back. Much like conventional imaging, ToF cameras suffer from the trade-off between depth of field (DOF) and light throughput: larger apertures allow for more light collection but results in smaller depth of field. This is especially limiting in ToF systems since they are active and are limited by illumination power, which eventually limits performance in long-range imaging or imaging in strong ambient illumination (such as outdoors). Motivated by recent work in extended depth of field imaging for photography, we propose a focal-sweep based image acquisition methodology to increase depth-of-field and eliminate defocus blur. Our approach allows for a simple inversion algorithm to recover all-in-focus images which is validated through simulation and experiment. We demonstrate a proof-of-concept focal sweep time-of-flight acquisition system and show results for a real scene.

TABLE OF CONTENTS

LIST OF FIGURES

ABBREVIATIONS

ToF	Time-of-flight
DOF	Depth of field
SNR	Signal to Noise Ratio
ADMM	Alternating Direction Method of Multipliers
TV	Total Variation
TGV^2	Second-order Total Generalized Variation

CHAPTER 1

Introduction

Time-of-flight (ToF) sensors are becoming commonplace in many consumer products (popular examples include Google's Project Tango, Microsoft's Kinect, and Creative's Senz3D) and are being used widely in many traditional and non-traditional applications in computer vision and graphics (Bhandari *et al.*, 2014; Heide *et al.*, 2013). There are broadly two classes: pulse modulated ToF sensors and continuous-wave modulated ToF sensors. The scope of this report is restricted specifically to continuous-wave ToF cameras, which calculate depth by measuring the phase difference between the emitted and received optical signal. This class of ToF sensors has emerged as an efficient, low-cost, compact and versatile depth imaging solution. Section 1.1 provides a brief overview the working methodology of ToF cameras. A more elaborate overview can be found in M. Hansard and Horaud (2013).

Even though ToF cameras seem a promising technology for a wide variety of applications which require real-time 3D information, the current generation of ToF sensors suffer from poor spatial resolution, temporal variation and sensor noise (Fursattel *et al.*, 2015). The distance measurement also suffers from wiggling (Lefloch *et al.*, 2013), internal scattering (Karel *et al.*, 2012), and temperature related errors (Fursattel *et al.*, 2015). Development of ToF sensors have addressed these limitations with improved designs (Chiabrando *et al.*, 2010; Mure-Dubois and Hügli, 2007); however, light throughput remains a significant challenge. Because ToF cameras rely on active light sources, whose intensity cannot be increased indefinitely due to safety and power restrictions, time-of-flight cameras suffer from poor light throughput. For static scenes, one option is to increase exposure duration; however, for natural scenes that do involve either camera motion or subject motion, this results in motion blur. The integration time of the ToF senors also cannot be increased too much as it has to be short enough to allow real-time operation. Consequently, a compromise is struck and a lens with large numerical aperture is used to make best use of the available light at the expense of decreasing the depth of field (DOF) and increasing defocus blur. The non-linear image formation model of ToF cameras further aggravates the problem, leading to artifacts

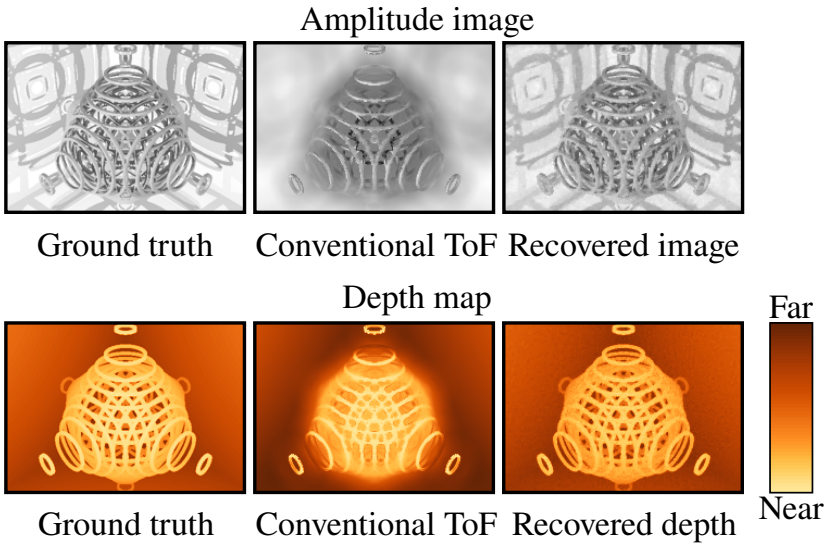

Figure 1.1: **Focal sweep imaging for handling large defocus blur in next generation time-of-flight (ToF) cameras:** For scenes with large depth variation (left) ToF cameras with small pixels (8 μm) will suffer from large defocus blur outside of the focus plane (center). We propose sweeping the focus over the scene during image exposure and deblurring the captured measurements before recovering the depth and amplitude (right). Top row: Measured amplitude images. Bottom Row: Computed depth map with the color map used throughout this paper.

like "flying pixels" around depth discontinuities and loss of texture detail. As the pixel sizes shrink in future generations of ToF sensors, the effect of defocus blur will only magnify, nullifying the anticipated gain in spatial resolution. The middle column in Figure 1.1 highlights the shortcoming of ToF systems with pixels 5 times smaller than current sensors. In this work, we propose an alternative configuration for ToF camera systems which considerably increases the DOF while retaining the light collection properties of lenses with high f-numbers.

1.1 Overview of continuous-wave ToF imaging

A continuous-wave ToF camera captures the depth of a scene point by measuring the phase delay ϕ of an optical path using the following relation:

$$z_p = \frac{c\phi}{4\pi f_M} \tag{1.1}$$

where f_M is the modulation frequency and c is the speed of light. To estimate ϕ with high precision, a TOF camera contains an active illumination source that is strobed

according to a periodic illumination signal.

Consider an active illumination source that projects a sinusoid, $cos(\omega t)$ onto a scene. Light reflects off of a point in the scene and returns to camera pixel p as $a_p cos(\omega t + \phi) + \beta$ where a_p is the amplitude of the reflected signal that reaches pixel p and β is the ambient illumination. ToF cameras capture the correlation between the reflected signal $a_p cos(\omega t + \phi) + \beta$ and a reference signal, which is usually of the form $cos(\omega t + \theta)$. The cross-correlation function evaluates to:

$$q(\theta, p) = \frac{a_p}{2} cos(\theta + \phi) + \beta \tag{1.2}$$

Four such correlation measurements $q_i(p); i = \{0, 1, 2, 3\}$ are captured with four different values of $\theta = i\frac{\pi}{2}; i = \{0, 1, 2, 3\}$. Using the quadrature measurements $q_i(p)$, the depth and amplitude can be computed as

$$\begin{aligned} z_p &= \tan^{-1}\left(\frac{q_1(p) - q_3(p)}{q_0(p) - q_2(p)}\right)\frac{c}{4f\pi} \\ a_p &= \sqrt{\left(q_0(p) - q_2(p)\right)^2 + \left(q_1(p) - q_3(p)\right)^2} \end{aligned} \tag{1.3}$$

This method is known as the "four bucket principle" as it takes four samples of the correlation function to estimate the phase and amplitude of the received optical signal.

1.2 Defocus blur in ToF cameras

Assuming the scene is in focus, the depth and image intensity (z_p and a_p) can be found using straightforward algebra and trigonometry. However, large aperture lenses restrict DOF and light reflecting from scene points outside of this region will be blurred together. Defocus blur is depth-dependent and hence, the point-spread-function (PSF) which characterizes the blur is also depth-dependent resulting in spatially varying blur across the image. The blurry quadrature measurements can be represented as the convolution $y_i(p) = K(z_p) * q_i(p)$, where $K(z_p)$ is the depth-dependent PSF and $y_i(p)$ are the blurry measurements. In the absence of motion blur, $K(z)$ can be precomputed and stored for each depth z. Sharp measurements of $q_i(p)$ can be recovered by deconvolving $y_i(p)$ with the appropriate PSF $K(z)$. However, we face a classic chicken and egg

problem. To compute the PSF, we first need to know the depth z_p, but to accurately compute z_p, we need to deconvolve $y_i(p)$.

In this work, we propose to use focal sweep (Cossairt and Nayar, 2010; Nagahara *et al.*, 2008; Häusler, 1972; Zhou *et al.*, 2012) to generate a depth-independent PSF by sweeping the focus plane over the entire scene during each exposure. The resulting PSF kernel K, is spatially-invariant and known *a priori* which leads to a straightforward non-blind deconvolution of y_i to recover the quadrature measurements q_i. (As the blur is uniform, we drop the pixel index p for convenience.)

1.3 Related work

1.3.1 Computational Depth of Field Extension

The use of computational imaging techniques, which involve the joint design of optics and processing algorithms, for extending depth of field of imaging systems is a well studied field. Focal sweep is one such well-known computational photography technique (Cossairt and Nayar, 2010; Zhou *et al.*, 2012) for extended depth of field imaging. Images captured with a large aperture suffer from a depth-dependent blur. In focal sweep imaging, either the distance between the lens and sensor (Nagahara *et al.*, 2008) or the subject and lens (Häusler, 1972) is varied at a constant rate during the exposure duration, and a single blurry image is captured. Nagahara *et al.* (2008) showed that focal-sweep images have a depth-independent point-spread-function. Hence, by estimating a single PSF and deconvolving the captured image a sharp, all-in-focus image can be obtained.

Image deblurring is inherently ill-posed. The frequency response of the defocus blur PSF exhibits nulls in the Fourier domain, precluding direct inversion. Coded apertures have been proposed as a means to overcome defocus blur for consumer cameras with large apertures (Veeraraghavan *et al.*, 2007; Levin *et al.*, 2007).

1.3.2 Defocus deblurring in ToF cameras

Godbaz *et al.* (2010) proposed a two-stage method for parametric blind deconvolution

of full-field continuous-wave ToF imaging. They estimate the lens parameters from a pair of Lidar measurements taken at different aperture settings, and then deconvolve these quadrature measurements, from which the final depth map is computed. Godbaz *et al.* (2011) applied the coded aperture technique to extend the depth of field for full-field continuous-wave Lidar imaging. The complex-domain Lidar measurement is iteratively deconvolved with a simple Gaussian derivative prior, while at each iteration the blur kernel of each pixel is updated according to the currently estimated Lidar image. Coded aperture improves the tractability of deconvolving y_i at the expense of sacrificing light throughput in an already light-limited imaging scenario.

Xiao *et al.* (2015) addressed the limited spatial resolution and defocus blur in time-of-flight sensors by analyzing the image formation model. As there is a loss of spatial resolution and depth-of-field information, they proposed to incorporate second-order total generalized variation as a prior for both amplitude and depth. In this formulation there are three unknowns: the depth-dependent PSF, the all-in-focus amplitude image, and the all-in-focus depth map. Alternating direction method of multipliers (ADMM) is used to solve for all-in-focus amplitude, and all-in-focus depth images. For simplicity, the PSF is pre-calibrated for each depth and the PSF used for each pixel is updated after updating the amplitude and depth. This algorithm is highly effective, and the state-of-the-art in the field, but it comes at a high computational cost.

CHAPTER 2

Focal Sweep Time-of-flight Imaging

The main contribution of this work is a system to remove defocus blur from ToF images using focal sweep to generate depth-independent blur. Figure 2.1 gives a high-level overview of the method proposed in this work. We use two deblurring algorithms for recovering all-in-focus ToF images. The first approach directly deblurs the raw quadrature measurements using a TV prior and uses the deblurred quadrature channels to obtain sharp amplitude and depth maps. On the other hand, the second approach directly estimates the latent amplitude and depth from the degraded measurements. The advantage of the second approach is that it allows us to apply separate regularizations on the amplitude and depth, and would also work for the next generation ToF cameras with multiple modulation frequencies, phases and exposures. We validate our approach via simulation and by capturing real data with a prototype system.

2.1 Capture method

We propose to capture focal sweep ToF measurements. During the capture of each quadrature channel, we move the lens while keeping the sensor static. The distance to be moved by the lens depends on the range of object distances in the scene. Each quadrature measurements is thus a focal sweep image, which makes the blur depth-independent for the given depth range (Nagahara *et al.*, 2008). So, unlike Xiao *et al.* (2015), we need not estimate the blur kernel at each pixel. In fact, given the depth range of the scene, sensor pixel size, focal length and aperture size, we can analytically compute the focal sweep PSF (Nagahara *et al.*, 2008).

$$\mathrm{PSF}(r,u) = \frac{uf}{(u-f)\sqrt{2\pi}rAsT}\left(\mathrm{erfc}\left(\frac{r}{\sqrt{2}b(0)}\right) + \mathrm{erfc}\left(\frac{r}{\sqrt{2}b(T)}\right)\right)$$

where u is the mean distance between the lens and the sensor, f is focal length, A is the

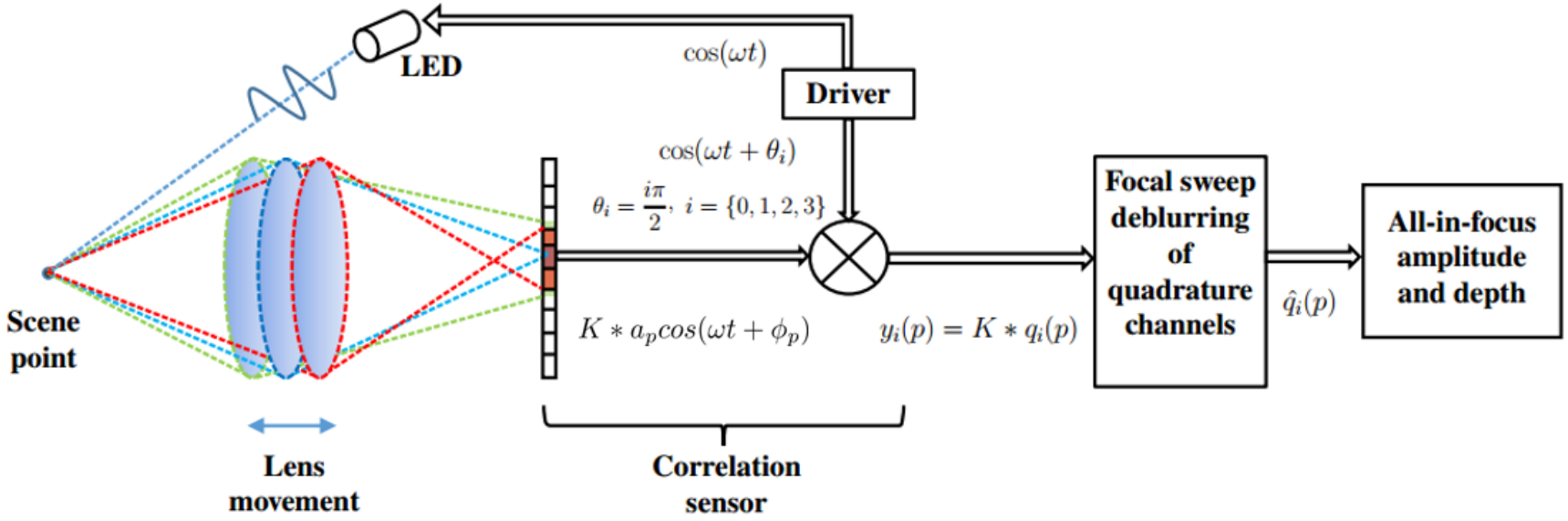

Figure 2.1: **Overview of the proposed method:** Each quadrature channel is captured by sweeping the focus over the scene depth range. As a result, the correlation measurements of the ToF sensor exhibit depth-invariant blur. All-in-focus amplitude and depth maps are then recovered from the captured ToF quadrature channels using the deblurring method in Section 2.2

aperture diameter, r is the distance of the pixel from the center of blur circle, s is the speed of the sensor, T is the exposure duration, and b is blur circle diameter at time t.

2.2 Deblurring method

2.2.1 Approach I

To obtain all-in-focus amplitude and depth images, we individually deblur each of the two independent channels h_{re} and h_{im}, which are in turn obtained from the four blurry quadrature measurements y_0, y_1, y_2, and y_3. The two independent measurements are given by $h_{re} = (y_0 - y_2)$ and $h_{im} = (y_1 - y_3)$. Note that the quadrature measurements are obtained by focal sweep and hence, blurred with the depth-independent focal sweep PSF (K). Therefore, the two independent measurements h_{re} and h_{im} are also the blurred versions of the corresponding sharp channels $X_{re} = a\cos(\phi)$ and $X_{im} = a\sin(\phi)$. We then find estimates of the sharp channels using non-blind deconvolution with a prior to regularize the total variation norm:

$$\widehat{X_{re}} = \text{argmin}_{X_{re}} ||h_{re} - K * X_{re}||^2 + \lambda ||X_{re}||_{TV},$$

with a similar formulation for $\widehat{X_{im}}$. Finally, we obtain the sharp amplitude and depth using equations (1.3) with appropriate substitutions of $\widehat{X_{re}}$ for $q_0 - q_2$ and $\widehat{X_{im}}$ for $q_1 - q_3$.

2.2.2 Approach II

In this deblurring method, we use the same optimization framework as Xiao *et al.* (2015) to compute the all-in-focus amplitude and depth map directly from the focal sweep measurements. The algorithm however becomes much simpler as we now have a depth independent blur kernel and do not require kernel update in each iteration. Following the framework of Xiao *et al.* (2015), we use second-order total generalized variation (TGV^2) prior for both all-in-focus depth and amplitude:

$$(a, z) = \arg\min_{a,z} ||h_{re} - K * X_{re}||^2 + ||h_{im} - K * X_{im}||^2 + \phi(a) + \psi(z)$$

$$X_{re} = a\cos\theta(z); \quad X_{im} = a\sin\theta(z) \tag{2.1}$$

where a is the ground truth amplitude, z is the ground truth scene depth, K is the depth-independent focal sweep blur matrix, b_r and b_i are the sensor measurements, and $\theta(z) = 4\pi f z/c$ is the phase delay that depends on the scene depth, modulation frequency f and the speed of light c. $\phi(a)$ and $\psi(z)$ are the TGV^2 regularization terms and are given by:

$$\begin{aligned}\phi(a) &= \min_y \lambda_1||\nabla a - y||_1 + \lambda_2||\nabla y||_1 \text{ and} \\ \psi(z) &= \min_x \tau_1||\nabla z - x||_1 + \tau_2||\nabla x||_1.\end{aligned} \tag{2.2}$$

We split the above optimization procedure and alternatively update the amplitude and depth, which are solved for using the Alternating Direction Method of Multipliers (ADMM - Boyd *et al.* (2011)).

2.3 Results

In this section, we demonstrate our proposed technique using simulated scenes and experimental data collected from a prototype camera detailed in Kadambi *et al.* (2013). With the availability of all-in-focus depth and amplitude images, we can perform post capture refocusing and artistic renderings such titled depth-of-field imaging, which is detailed at the end of this section.

2.3.1 Simulation experiments

We first obtain the focal sweep quadrature images by simulating our prototype ToF camera which has a pixel size of 45 μm, and is fitted with a $f/1.4$ lens.

Figure 2.2 shows the expected results of using our proposed camera with current

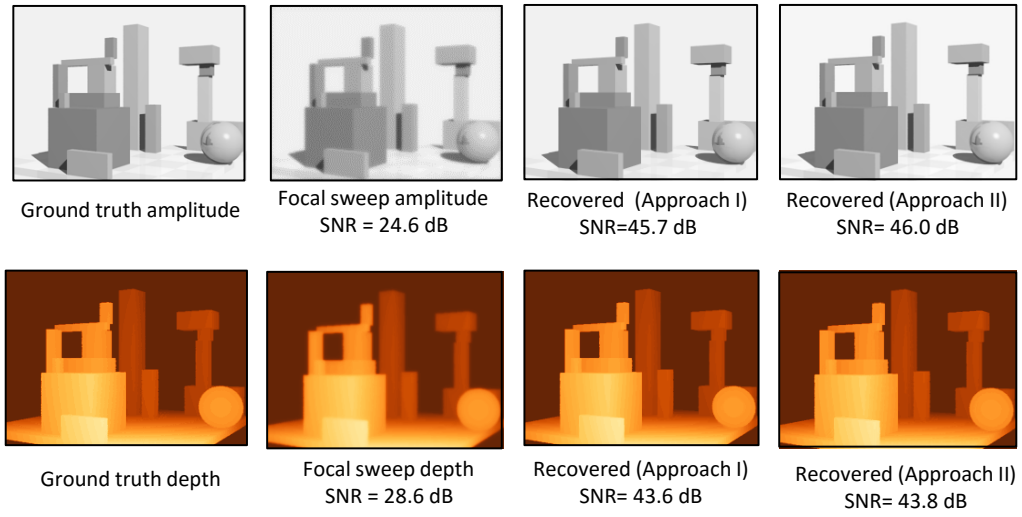

Figure 2.2: **Simulation of recovering all-in-focus ToF images using focus sweep:** For a known a scene and depth map we simulate capturing focal sweep ToF images. Using the captured images results in amplitude and depth images with a uniform blur. All-in-focus amplitude and depth images recovered by deblurring the focal sweep measurements using the two algorithms in Section 2.2

generation ToF sensors. We simulate focal sweep during acquisition of each of the quadrature measurements. Directly using the resulting images yields amplitude and depth measurements that have a uniform blur as shown in Figure 2.2 (b). All-in-focus amplitude and depth images in Figure 2.2 (c) and (d) are recovered from the blurry quadrature measurements using the two algorithms outlined in Section 2.2. It is seen that the second approach produces better quality amplitude and depth maps compared to the first method. This is due to the fact that the second method seeks to estimate the latent amplitude and depth directly from the raw measurements, enabling us to apply separate regularizations to the amplitude and depth. The second method is also more suitable for next-generation ToF cameras with multiple modulation frequencies, phases and exposures. However, the second approach takes around 10 times longer to run compared to Approach I.

The current pixel size of ToF cameras are quite large $45\ \mu$m and the sensor resolution is low, (e.g. 153×120 for our PMD sensor). However, with advances in ToF sensor technology we can expect future generations of ToF cameras to have smaller pixel size and higher resolution. This will result in increased defocus blur; the need for computational techniques to recover sharp images in these sensors will be more pronounced. This will result in increased defocus blur and the need for computational

techniques to recover sharp images in these sensors will be apparent. To simulate the effect smaller pixels will have and to gauge the performance of our algorithm on future generations of ToF cameras, we consider a pixel size to 8 μm in our next simulation experiment. Figure 2.3 shows our simulation results. The virtual scene in Figure 2.3(a) has a depth range of $[0.48, 0.85]$ meters. We introduce Gaussian noise to the quadrature measurements amounting to an input SNR of approximately 40 dB. Figure 2.3(b) shows a conventional ToF image captured by a ToF camera which has a pixel size of 8 μm, and is fitted with a $f/1.4$ lens focused in the middle of the scene. It is degraded by significant defocus blur due to limited DOF. Using a state-of-the-art ToF defocus deblurring algorithm proposed by Xiao *et al.* (2015) results in Figure 2.3(c). We obtain the focal sweep quadrature images by simulating our prototype ToF camera. Figure 2.3(d) shows the amplitude and depth maps obtained from the focal sweep measurements. All-in-focus amplitude and depth maps recovered by our method (using the first approach) from the focal sweep images are shown in Figure 2.3(e). Our deblurring algorithm requires an estmate of the depth-independent PSF. To estimate the focal sweep PSF, we simulate a point light source in the center of the scene depth range and compute the blur undergone by it during focal sweep. This is taken as the blur PSF estimate for the entire scene. Our algorithm then uses the depth-invariant PSF and does a non-blind deconvolution with TV regularization on the quadrature channels to recover sharp amplitude and depthmap of the scene. It is seen the proposed method significantly increases the DOF and produces superior quality outputs with better SNR compared to Xiao *et al.* (2015).

2.3.2 Real experiments

Capturing a focal sweep image requires the focus to varying continuously during image acquisition. We build a proof-of-concept prototype system using a ToF imager outlined in Kadambi *et al.* (2013). Similar to the process described in Nagahara *et al.* (2008), a large aperture lens ($f/1.4$) is mounted on a translation stage to vary the distance between the sensor and lens. A sequence of 26 images is captured by increasing separation distance of the lens and sensor in 50 μm increments to create a focal stack. A focal sweep image is then formed by integrating the stack into a single blurry image for each of the four quadrature measurements.

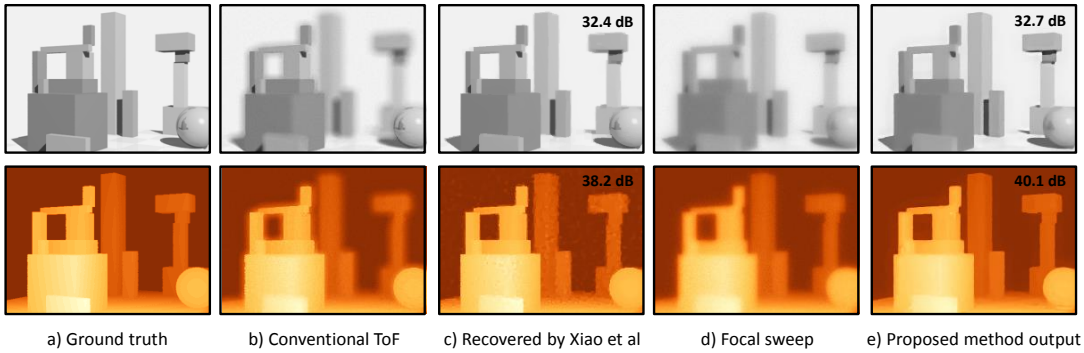

Figure 2.3: **Comparison with prior method by Xiao *et al.* (2015) on simulated scene:** a) Ground truth ampitude and depth map of the simulated scene. b) Mid-focus conventional ToF images degraded by defocus blur c) Amplitude and depth maps recovered from (b) using the algorithm proposed by Xiao *et al.* (2015) d) Using the captured focal sweep measurements results in amplitude and depth images with a uniform blur. e) All-in-focus amplitude and depth images recovered by deblurring the focal sweep measurements using our method.

Figure 2.4 depicts a scene captured with our setup while Figure 2.4 (a-c) shows the corresponding amplitude images and depth maps captured at near-, mid-, and far-focus positions. Notice that defocus blur significantly reduces image quality for objects outside of the DOF. By deblurring each of the quadrature measurements and following the procedure in Section 2.2, we recover an all-in-focus amplitude image and depth map (Figure 2.4 (d)). PSF calibration for the experimental data is determined a priori by summing the blur response of a point source as the camera focus is swept through the extended DOF of interest. Detailed outsets below each of the amplitude measurements shows image patches from three depths, corresponding to the focal planes in Figure 2.4 (a-c). Only after deblurring the focal sweep quadrature measurements are all three patches sharp, and each is of comparable quality to the corresponding in-focus patches.

2.3.3 Post-capture refocusing and titled DOF

Once we obtain all-in-focus amplitude and depth images, we can render the scene with different lens and aperture settings computationally without a physical lens. In Figure 2.5 (a-b), we illustrate the ability to tilt the lens and render an artistic scene using color images to act as visual aids. This may be useful when we want to obtain all-in-focus images of tilted planes or surfaces in real-world scenes. Figure 2.5(b) shows the rendering effect when we tilt the virtual lens to focus along the red, striped plane

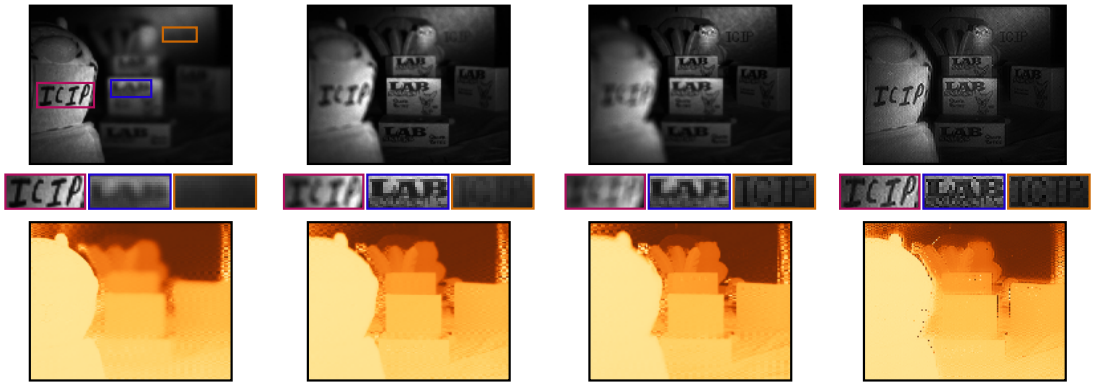

Figure 2.4: **Recovering all-in-focus images for a real ToF system** As a proof-of-concept we use the ToF system described in Kadambi *et al.* (2013) with an $f/1.4$ lens to capture a sequence of images of the scene shown in (a-c). A sequence of 26 measurements is recorded by increasing lens-sensor separation by 50 μm between positions.. Integrating these measurements yields the comparable focal sweep data. (d) Deblurring the quadrature measurements provides sharp all-in-focus images. Top row: Amplitude images. Middle row: Detail views of three patches located in the near-, mid-, and far-field. Bottom row: Depth images.

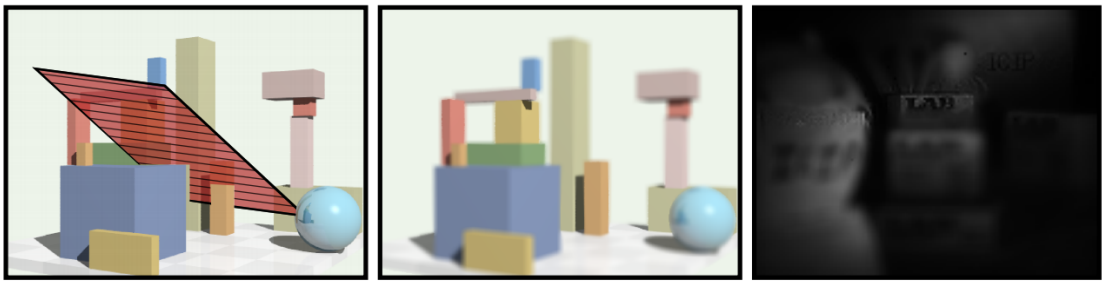

Figure 2.5: **Post-capture tilted plane refocusing:** Left: Ground truth scene. Middle: The scene is refocused along an arbitrary plane (red striped plane shown in ground truth). Color images are used to help visualize the rendering. Right: The recovered scene from Figure 2.4(d) is refocused along a nearly horizontal focal plane.

in Figure 2.5(a). In Figure 2.5(c), the all-in-focus result of Figure 2.4(d) is refocused along a nearly horizontal focal plane. Only with sharp depth maps are such post-capture renderings possible without resorting to bulky specialized equipment.

CHAPTER 3

Conclusions

3.1 Summary

In this work, we have presented a novel methodology for depth of field extension in ToF cameras using focal sweep. Two algorithms have been used for performing a non-blind deconvolution of the focal sweep quadrature measurements to obtain all-in-focus amplitude and depth maps.

The first approach discussed in Section 2.2.1 directly deblurs the quadrature measurements using a TV norm regularization. This algorithm is fast and allows real-time operation. The simplicity of this recovery algorithm will enable straightforward scale-up to handle increasing spatial-resolution and defocus blur in future generations of ToF cameras.

The second algorithm discussed in Section 2.2.2, whose optimization framework is adopted with suitable modification from Xiao *et al.* (2015), estimates the sharp amplitude and depth maps directly from the focal sweep quadrature measurements in a single shot. Our modified algorithm is much faster than Xiao *et al.* (2015) as the focal sweep blur kernel is depth-independent and need not be updated based on the estimated depth in each iteration of the algorithm. An advantage of the second method is that it can easily incorporate multiple modulation frequencies, phases and exposures in the deblurring process, thus making it suitable for next-generation ToF cameras. However, as this algorithm tries to solve the optimization problem in a single shot, it involves non-linear depth update steps and is computationally very expensive.

Though the recovered amplitude and depth maps from the second algorithm have a slightly better SNR, its runtime is an order of magnitude higher than the first approach. Depending on the application, a suitable choice of algorithm can be made based on the trade-off between output SNR and runtime.

3.2 Future work

In this work, we have incorporated TV regularization for deblurring the quadrature measurements in the first approach as we found that it gave good results on a wide range of scenes. It would be interesting to study other techniques such as BM3D or TGV^2 to see if there are better priors for time-of-flight quadrature measurements which could be used to obtain much higher SNR outputs.

Once a ToF focal stack is obtained, many other applications are possible such as novel view synthesis of both amplitude and depth maps, which has not yet been explored in the context of time-of-flight cameras. This could be an interesting avenue for further research as well.

REFERENCES

1. **Bhandari, A.**, **C. Barsi**, **R. Whyte**, **A. Kadambi**, **A. J. Das**, **A. Dorrington**, and **R. Raskar**, Coded time-of-flight imaging for calibration free fluorescence lifetime estimation. *In Imaging and Applied Optics 2014*. Optical Society of America, 2014. URL http://www.osapublishing.org/abstract.cfm?URI=ISA-2014-IW2C.5.

2. **Boyd, S.**, **N. Parikh**, **E. Chu**, **B. Peleato**, and **J. Eckstein** (2011). Distributed optimization and statistical learning via the alternating direction method of multipliers. *Foundations and Trends® in Machine Learning*, **3**(1), 1–122.

3. **Chiabrando, F.**, **D. Piatti**, and **F. Rinaudo** (2010). Sr-4000 tof camera: further experimental tests and first applications to metric surveys. *Int. Arch. Photogramm. Remote Sens. Spatial Inf. Sci*, **38**(5), 149–154.

4. **Cossairt, O.** and **S. Nayar**, Spectral focal sweep: Extended depth of field from chromatic aberrations. *In Computational Photography (ICCP), 2010 IEEE International Conference on*. IEEE, 2010.

5. **Fursattel, P.**, **S. Placht**, **C. Schaller**, **M. Balda**, **H. Hofmann**, **A. Maier**, and **C. Riess** (2015). A comparative error analysis of current time-of-flight sensors.

6. **Godbaz, J. P.**, **M. J. Cree**, and **A. A. Dorrington** (2010). Blind deconvolution of depth-of-field limited full-field lidar data by determination of focal parameters. URL http://dx.doi.org/10.1117/12.838553.

7. **Godbaz, J. P.**, **M. J. Cree**, and **A. A. Dorrington**, Extending amcw lidar depth-of-field using a coded aperture. *In Computer Vision–ACCV 2010*. Springer, 2011, 397–409.

8. **Häusler, G.** (1972). A method to increase the depth of focus by two step image processing. *Optics Communications*, **6**(1), 38–42.

9. **Heide, F.**, **M. B. Hullin**, **J. Gregson**, and **W. Heidrich** (2013). Low-budget transient imaging using photonic mixer devices. *ACM Trans. Graph.*, **32**(4), 45:1–45:10. ISSN 0730-0301. URL http://doi.acm.org/10.1145/2461912.2461945.

10. **Kadambi, A.**, **R. Whyte**, **A. Bhandari**, **L. Streeter**, **C. Barsi**, **A. Dorrington**, and **R. Raskar** (2013). Coded Time of Flight Cameras : Sparse Deconvolution to Address Multipath Interference and Recover Time Profiles. *ACM Transactions on Graphics*, **32**(6), 1–10. ISSN 07300301. URL http://web.media.mit.edu/~achoo/nanophotography/$\delimiter"026E30F$nhttp://dl.acm.org/citation.cfm?id=2508363.2508428.

11. **Karel, W.**, **S. Ghuffar**, and **N. Pfeifer** (2012). Modelling and compensating internal light scattering in time of flight range cameras. *The Photogrammetric Record*, **27**(138), 155–174.

12. **Lefloch, D.**, **R. Nair**, **F. Lenzen**, **H. Schäfer**, **L. Streeter**, **M. J. Cree**, **R. Koch**, and **A. Kolb**, Technical foundation and calibration methods for time-of-flight cameras. *In Time-of-Flight and Depth Imaging. Sensors, Algorithms, and Applications*. Springer, 2013, 3–24.

13. **Levin, A.**, **R. Fergus**, **F. Durand**, and **W. T. Freeman**, Image and depth from a conventional camera with a coded aperture. *In ACM Transactions on Graphics (TOG)*, volume 26. ACM, 2007.

14. **M. Hansard, S. L., O. Choi** and **R. Horaud** (2013). Time-of-flight cameras.

15. **Mure-Dubois, J.** and **H. Hügli**, Real-time scattering compensation for time-of-flight camera. *In Proceedings of the ICVS Workshop on Camera Calibration Methods for Computer Vision Systems*. 2007.

16. **Nagahara, H.**, **S. Kuthirummal**, **C. Zhou**, and **S. K. Nayar**, Flexible depth of field photography. *In Computer Vision–ECCV 2008*. Springer, 2008, 60–73.

17. **Veeraraghavan, A.**, **R. Raskar**, **A. Agrawal**, **A. Mohan**, and **J. Tumblin** (2007). Dappled photography: Mask enhanced cameras for heterodyned light fields and coded aperture refocusing. *ACM Trans. Graph.*, **26**(3), 69.

18. **Xiao, L.**, **F. Heide**, **M. O'Toole**, **A. Kolb**, **M. B. Hullin**, **K. Kutulakos**, and **W. Heidrich**, Defocus deblurring and superresolution for time-of-flight depth cameras. *In Proceedings of the IEEE Conference on Computer Vision and Pattern Recognition*. 2015.

19. **Zhou, C.**, **D. Miau**, and **S. K. Nayar** (2012). Focal sweep camera for space-time refocusing.

LIST OF PAPERS BASED ON THESIS

1. **Sagar Honnungar, Jason Holloway, Adithya Pediredla, Ashok Veeraraghavan,** and **Kaushik Mitra**. Focal Sweep for Large Aperture Time-of-flight Cameras. *International Conference on Image Processing*, 2016.